

Development of Low-Loss Broad-Band Planar Baluns Using Multilayered Organic Thin Films

Andy C. Chen, *Member, IEEE*, Anh-Vu Pham, *Senior Member, IEEE*, and Robert E. Leoni III, *Member, IEEE*

Abstract—This paper presents the design and development of a low-loss and wide-band width multilayered Marchand balun. The balun has been implemented using printed circuit board materials with integrated multilayered organic thin films. We have designed the top layer transmission lines on twin-thickness organic thin films to achieve low loss and wide bandwidth for the balun. The experimental results demonstrate that the balun achieves less than 0.5–0.7 dB insertion loss throughout the 4–20-GHz operation bandwidth. The phase and amplitude imbalances are less than 5° and 0.5 dB, respectively. Time-domain measurement results demonstrate that the balun has negligible dispersion.

Index Terms—Baluns, broad-band, dispersion, imbalance, microwave, thin film, time domain.

I. INTRODUCTION

THE MARCHAND balun [1] is a popular RF/microwave component used in broad-band advanced communication systems designs. When used in balanced mixers and push–pull amplifiers, baluns convert unbalanced signals into balanced signals and vice versa. The Marchand compensated balun was implemented originally in coaxial cables, and later converted into planar structures suitable for miniaturized system integration. Planar baluns have been implemented using various type of transmission lines, including coupled microstrip lines [2], [3], coupled coplanar waveguide (CPW) lines [4], and multilayered broadside-coupled microstrip lines [5]–[9]. The single-layer edge-coupled microstrip and CPW baluns are easier to fabricate, but have smaller bandwidth ratios, with values lower than 2.7 : 1 reported to date. Multilayered planar baluns, on the other hand, are more complicated to fabricate, but they provide larger bandwidth ratios.

In this paper, we report the development of a printed circuit, multilayered, and coax-like version of the Marchand balun that covers a 4–20-GHz operation bandwidth. This multilayered balun design is derived from that originally proposed by Bawer and Wolfe [10], and has been implemented on a printed circuit board with polymer thin films on top to allow for the integration of multilayer transmission lines. The balun consists of two sections of broadside-coupled microstrip lines, and has wide metal traces to reduce conduction loss. Wide metal traces have been

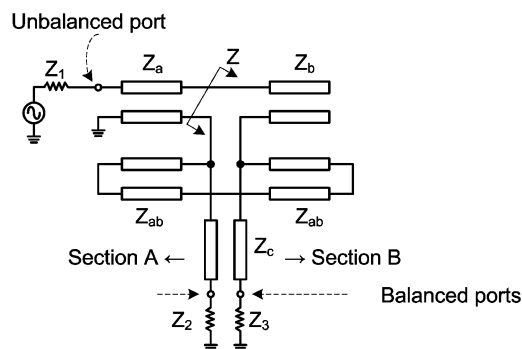


Fig. 1. Equivalent TEM transmission-line model of the compensated Marchand balun.

used in baluns to reduce conduction loss by Tutt *et al.* [5]. This concept is further expanded here with the usage of multithickness dielectrics in order to avoid the drawback of a smaller bandwidth caused by a thick thin film. We have developed one section of the coupled lines with its top microstrip transmission line on a thick polymer layer to increase the strip width and minimize loss [11], while the other section's top microstrip transmission line is on a thin layer to maintain low impedance for wide bandwidth performance. Sections II and III describe the design and analysis of the balun; whereas Section IV discusses the origins of phase imbalance and presents an equivalent-circuit model for the balun. The model is based on normal mode and physical parameters, and its simulation results agree well with experimental results. Section V shows the experimental results for the balun conducted in both the frequency and time domains. The measured results demonstrate that the balun has an insertion loss of less than 0.5 dB from 4 to 17 GHz, less than 0.7 dB from 17 to 20 GHz, and 0.5 dB and 5° of amplitude and phase imbalances, respectively. To the best of our knowledge, this is the widest bandwidth achieved for a planar balun while maintaining a lowest possible insertion loss, as compared to [9]. Time-domain measurements show an indistinguishable amount of pulse widening of a Gaussian-like pulse passing through the balun, demonstrating the balun achieving minimal dispersion.

II. IDEAL TRANSMISSION-LINE MODEL

The design of the balun starts with the equivalent TEM wave mode transmission-line model of the Marchand balun, as shown in Fig. 1. The following assumptions are applied to the ideal model to simplify the initial stage design process. First, the balun is constructed in a homogeneous medium. Secondly, equal transmission-line lengths of a quarter-wavelength at the center frequency of the operation band are used. Thirdly, the

Manuscript received April 5, 2005; revised June 24, 2005. This work was supported by the Raytheon Company, by the University of California under a Discovery Grant, and by the National Science Foundation under CAREER Award ECS-0300649.

A. C. Chen and A.-V. Pham are with the Electrical and Computer Engineering Department, University of California at Davis, Davis, CA 95616 USA (e-mail: acchen@ucdavis.edu; pham@ece.ucdavis.edu).

R. E. Leoni III is with the RF Components Division, Raytheon Company, Andover, MA 01810 USA.

Digital Object Identifier 10.1109/TMTT.2005.857102

transmission lines are well isolated and operate in a single TEM propagation mode.

A. Bandwidth Calculation

Based on the above assumptions, the bandwidth of the TEM balun has been traditionally calculated [12] by matching Z with the source impedance Z_1

$$Z = -jZ_b \cot \theta_b + \frac{j2RZ_{ab} \tan \theta_{ab}}{R + j2Z_{ab} \theta_{ab}} \quad (1)$$

where Z is the impedance looking into the balun at the gap point, as shown in Fig. 1, and R is the sum of the load impedances Z_2 and Z_3 . The bandwidth can also be found from an explicit expression of S_{21} derived from the TEM model of the balun

$$S_{21, \text{balun}} = -S_{31, \text{balun}} = \frac{N(\theta)}{D(\theta)} \quad (2a)$$

where $N(\theta)$ and $D(\theta)$ are

$$\begin{aligned} N(\theta) = & \left[-(Z_a + Z_b)(Z_{ab} + Z_2) \cos^3 \theta \right. \\ & + (Z_{ab}Z_a + 3Z_{ab}Z_b + Z_aZ_2) \cos \theta \\ & + j(Z_aZ_2 + Z_2Z_b + 2Z_{ab}Z_2 + 2Z_{ab}Z_b) \cos^2 \theta \sin \theta \\ & \left. + jZ_{ab}(Z_a + 2Z_2) \sin \theta \right] \cdot 2\sqrt{Z_2Z_aZ_{ab}} \sin^2 \theta \end{aligned} \quad (2b)$$

$$\begin{aligned} D(\theta) = & Z_{ab}^2 (Z_a^2 + 4Z_aZ_2 + 4Z_2^2) \\ & + \left[(Z_b^2 - 2Z_a^2 - 8Z_2^2 - 8Z_2Z_a) Z_{ab}^2 \right. \\ & \left. + (Z_a^2 - 4Z_{ab}Z_b) Z_2^2 \right] \cos^2 \theta \\ & + \left[(4Z_2^2 - Z_b^2 + 4Z_2Z_a + Z_a^2) Z_{ab}^2 \right. \\ & \left. + (Z_b^2 - Z_a^2 + 4Z_{ab}Z_b) Z_2^2 \right] \cdot \cos^4 \theta. \end{aligned} \quad (2c)$$

Equation (2a)–(2c) assumes the balanced ports are terminated with equal load impedances $Z_3 = Z_2$, all transmission lines are of equal electrical lengths $\theta_{ab} = \theta_a = \theta_b = \theta$, and the value of Z_a is matched to Z_1 . With the aid of (2a) and (2c), one can determine the bandwidth of the balun by constraining S_{21} to be larger than a minimum design value

$$S_{21} \geq S_{21, \text{min}} \quad (3)$$

The widest bandwidth that can be achieved and predicted by the TEM model of the balun is determined by the characteristic impedances Z_a , Z_b , and Z_{ab} , together with termination impedances Z_1 , Z_2 , and Z_3 .

B. Amplitude and Phase Imbalance

Amplitude and phase imbalances of the balun's balanced ports will cause the conversion of differential-mode signals into common-mode signals. Phase imbalance is the amount of deviation from the ideal case of an exact 180° phase difference from S_{21} to S_{31} . For the ideal TEM balun, as can be seen from (2a)–(2c), amplitude and phase imbalances are exactly zero, despite the operation frequency. Analysis of phase and amplitude imbalances will be detailed in Section IV.

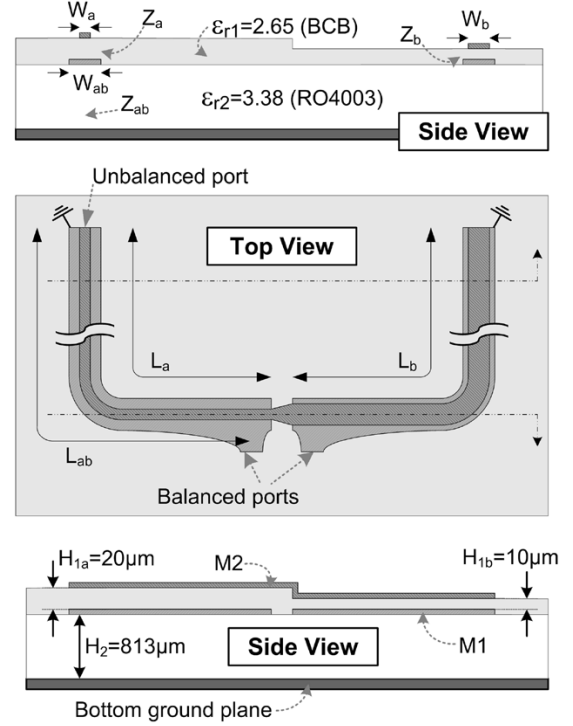


Fig. 2. Schematic top and side views of the twin-thickness dielectric thin-film balun.

III. DESIGN

The multilayer construction of the balun to be designed is shown in Fig. 2. The metal 2 (M2) layer trace having width W_a (W_b), together with the metal 1 (M1) layer trace having width W_{ab} form microstrip transmission line Z_a (Z_b). Metal 1 layer traces W_{ab} and the bottom ground plane form microstrip transmission lines Z_{ab} . Notice that the ground return signal for the microstrip line Z_a is shared with the signal trace of microstrip line Z_{ab} ; this is the basic difference of this type of broadside coupled lines balun from the edge coupled transmission-line designs listed in [2] and [3], where ground return signals for both transmission lines Z_a (Z_b) and Z_{ab} are merged into the same backside ground plane.

A. Single Dielectric Thin-Film Thickness

The transmission lines with their characteristic impedances determined using the procedure outlined in Section II are now implemented with microstrip transmission lines. The relation among bandwidth, conduction loss, and dielectric thickness is plotted as shown in Fig. 3.

Insertion loss of the entire balun is dominated by the conduction loss of the narrowest line, which is microstrip line Z_a . Moreover, current densities are also the highest within microstrip line Z_a . Conduction loss of the microstrip line with length L_a can be approximated by [13], [14]

$$\alpha_c = 8.686 \frac{R_s L_a}{Z_0 W} = 8.686 \frac{\sqrt{\omega \mu_0 / 2 \sigma}}{Z_0 W} \cdot L_a \quad (\text{dB}). \quad (4)$$

From Fig. 3, one can rapidly evaluate the optimum dielectric thin-film thickness to be used. Small thickness values lead to

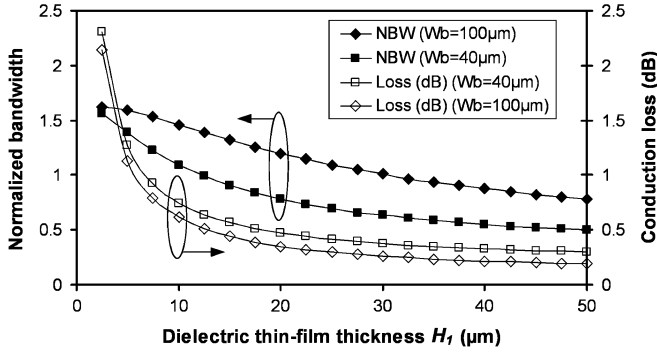


Fig. 3. Normalized bandwidth (NBW) of a single-layer thin-film balun and conduction loss versus dielectric thin-film thickness. The normalized bandwidth is defined to be $(f_H - f_L)/f_0$ with f_0 being the passband center frequency and f_H and f_L being the high and low cutoff frequencies of the passband where $S_{21} = S_{21,\min}$ occurs. Bandwidth was calculated using (3), while conduction loss was calculated using (4). Values used were fixed at $Z_a = 50 \Omega$, $Z_{ab} = 144 \Omega$, and $Z_2 = Z_3 = 35 \Omega$.

larger bandwidth, but also increases the conduction loss drastically due to the narrow lines of microstrip Z_a . A thickness of 10–25 μm is optimal for the single thin-film thickness case, which can typically be implemented with polymer dielectrics such as bisbenzocyclobutene (BCB).¹

B. Twin Dielectric Thin-Film Thickness

In order to decouple the tradeoff between bandwidth and conduction loss, as seen in Fig. 3, one must give the design an extra degree of freedom. Since the value of characteristic impedance Z_a is normally set to 50 Ω and determined by the W_a/H_{1a} ratio of the line, it is independent of the exact dielectric thickness. Hence, a thicker dielectric thin film can be assigned for the construction of transmission line Z_a to specifically reduce conduction loss, while keeping a thin dielectric for microstrip line Z_b to maintain the bandwidth.

C. Dielectric Material Selection

The selection of dielectric materials and their corresponding dielectric constants directly alter the effective electrical lengths for each of the two coupled transmission-line sections. The dielectric materials were chosen to have near identical dielectric constants to meet the homogenous assumption listed earlier. The exact effect of using different dielectric constant materials is evaluated using the c/π -mode model discussed in Section IV with results shown in Fig. 4. Materials having large dielectric-constant differences for the top and bottom dielectrics cause a large v_π/v_c ratio and longer electrical lengths for c -mode propagations, shrinking the bandwidth of the balun since not all transmission lines are equal to a quarter-wavelength at the center frequency in their respective modes.

IV. MULTIMODE ANALYSIS

A. Multimode Propagation and Imbalance of the Balun

Metal traces on the two layers M2 and M1 together with the back ground plane form a pair of broadside coupled microstrip lines capable of supporting two distinct propagation modes. The

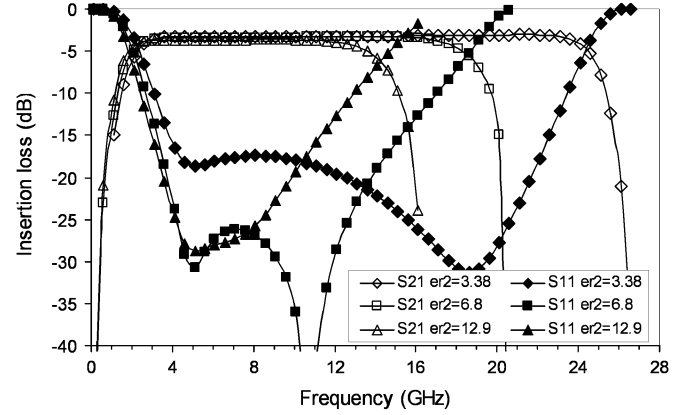


Fig. 4. Effect of bottom dielectric material selection on balun's bandwidth. Value of ϵ_{r1} was fixed at 2.65, while ϵ_{r2} is varied from 3.38 to 6.8 and 12.9. All other parameters are fixed with $H_{1a} = 20 \mu\text{m}$, $H_{1b} = 10 \mu\text{m}$, $H_2 = 813 \mu\text{m}$, $W_a = 42 \mu\text{m}$, $W_{ab} = 182 \mu\text{m}$, $L_a = 3575 \mu\text{m}$, and $L_b = 3575 \mu\text{m}$.

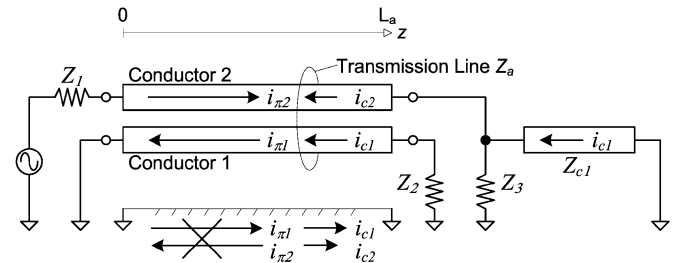


Fig. 5. Representative flow of c - and π -mode currents in a multilayered balun.

two modes are designated as the c - (in-phase) and π -mode (antiphase), first analyzed by Tripathi [15]. For the compactness of the analysis presented below, two new parameters IR_c and IR_π are introduced as the following:

$$v_1(z) = (A_1 e^{-\gamma_c z} + A_2 e^{\gamma_c z}) + (A_3 e^{-\gamma_\pi z} + A_4 e^{\gamma_\pi z}) \quad (5a)$$

$$v_2(z) = R_c (A_1 e^{-\gamma_c z} + A_2 e^{\gamma_c z}) + R_\pi (A_3 e^{-\gamma_\pi z} + A_4 e^{\gamma_\pi z}) \quad (5b)$$

$$i_1(z) = Y_{c1} (A_1 e^{-\gamma_c z} - A_2 e^{\gamma_c z}) + Y_{\pi1} (A_3 e^{-\gamma_\pi z} - A_4 e^{\gamma_\pi z}) = i_{c1} + i_{\pi1} \quad (5c)$$

$$i_2(z) = IR_c Y_{c1} (A_1 e^{-\gamma_c z} - A_2 e^{\gamma_c z}) + IR_\pi Y_{\pi1} (A_3 e^{-\gamma_\pi z} - A_4 e^{\gamma_\pi z}) = i_{c2} + i_{\pi2} \quad (5d)$$

where $i_1(z)$ and $i_2(z)$ are the total currents flowing on conductors 1 and 2, respectively (Fig. 5), γ_c and γ_π are the c - and π -mode phase constants, A_1 – A_4 are the intensities of the respective incident and reflected c and π modes, and Y_{c1} and $Y_{\pi1}$ are the characteristic admittances of conductor 1 for the two modes. The ratios of currents in the two modes are defined to be

$$IR_c = \frac{i_{c2}}{i_{c1}} = \frac{Y_{c2} R_c}{Y_{c1}} = -\frac{1}{R_\pi} \quad (6a)$$

and

$$IR_\pi = \frac{i_{\pi2}}{i_{\pi1}} = \frac{Y_{\pi2} R_\pi}{Y_{\pi1}} = -\frac{1}{R_c}. \quad (6b)$$

The c - and π -mode currents of the two conductors can be visualized in Fig. 5 to explain the operation of the multilayered balun. Conductor 2 is located on top of conductor 1 in case of

¹[Online]. Available: <http://www.dow.com/cyclotene/index.htm>

a pair of broadside coupled lines. The π -mode currents $i_{\pi 1}$ and $i_{\pi 2}$ are opposite in directions, whereas the c -mode currents i_{c1} and i_{c2} flow in the same direction by definition of in-phase. The ground return currents for $i_{\pi 2}$ and $i_{\pi 1}$ perfectly cancel out each other in the back ground plane when $IR_{\pi} = -1$, effectively making conductor 1 the ground trace for microstrip transmission line Z_a with the signal trace on conductor 2.

Ratios IR_c and IR_{π} are dependent on the coupled lines cross-sectional structure as

$$IR_c = -\frac{z_m(\gamma_c^2 - z_{11}y_{11} - z_{22}y_{22} - z_m y_m) - z_{22}(z_{11}y_m)}{z_{22}(\gamma_c^2 - z_{22}y_{22} - 2z_m y_m) - z_m(z_{11}y_{11})} \quad (7a)$$

$$IR_{\pi} = -\frac{z_{11}(\gamma_{\pi}^2 - z_{11}y_{11} - 2z_m y_m) - z_m(z_m y_{22})}{z_m(\gamma_{\pi}^2 - z_{11}y_{11} - z_{22}y_{22} - z_m y_m) - z_{11}(z_{22}y_m)} \quad (7b)$$

where $z_{jj}(j = 1, 2)$ and $y_{jj}(j = 1, 2)$ are the self-impedance and admittance per unit length of lines 1 and 2, and z_m and y_m are the mutual impedance and admittance per unit length.

A special case occurs when the width of conductor 1, or W_{ab} , is set to infinite, where conductor 2 is completely shielded off from the back ground plane. In this case, $y_m = -j\omega c_m = j\omega c_{22} = y_{22}$ and $z_m = j\omega l_m = j\omega l_{11} = z_{11}$, where c_m , c_{22} , l_m , and l_{11} are the mutual capacitance and inductance and self-capacitance and inductance of the conductors per unit lengths, assuming lossless dielectrics and conductors. This leads to the result of $IR_c = 0$ ($i_{c2} = 0$) and $IR_{\pi} = -1$ ($i_{\pi 1} = -i_{\pi 2}$), indicating a complete elimination of the c -mode current on conductor 2. If we further assume that the open-stub line Z_b is replaced by a perfect short, and the section B side transmission line Z_{ab} is replaced by Z_{c1} , as in Fig. 5 such that currents i_{c1} on both sides are also cancelled out, a perfect balance of currents at the balanced ports is achieved, same as that of the ideal coaxial balun case.

As implied from (5), the exact amount of imbalance is a complex function of not only ratios IR_c and IR_{π} , phase velocities v_c and v_{π} (which are all dependent on the balun's cross-sectional structure and dimensions), but also a function of frequency and load terminations. Thus, one may expect the imbalances of the balun to worsen under severely mismatched loads at the balanced ports.

Fig. 6 shows the effects of material selection for the bottom dielectric. As ϵ_{r2} is increased from 2.65 to 12.9 while keeping $\epsilon_{r1} = 2.65$, the c - and π -mode phase velocities become more and more mismatched (larger v_{π}/v_c ratios). However, since the value of IR_c becomes closer to 0, the current i_{c2} on conductor 2 becomes more and more suppressed, and the phase imbalance actually decreases. Fig. 7 also demonstrates that phase imbalance is much more dependent on IR_c than on the v_{π}/v_c ratio. Different structures were analyzed to investigate their phase velocities and phase imbalances. As shown from this figure, balun structures using edge-coupled microstrip lines show a much higher amount of phase imbalance due to their higher IR_c values and c -mode intensities. The trait of higher phase imbalances for edge-coupled lines baluns is also observed from the measurement results in [16].

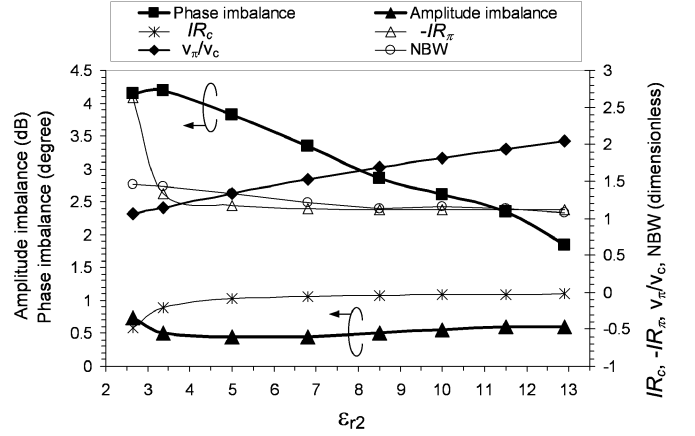


Fig. 6. Maximum in-band phase imbalance versus ϵ_{r2} for the broadside coupled balun. Simulation conditions are the same as those used for generating Fig. 4.

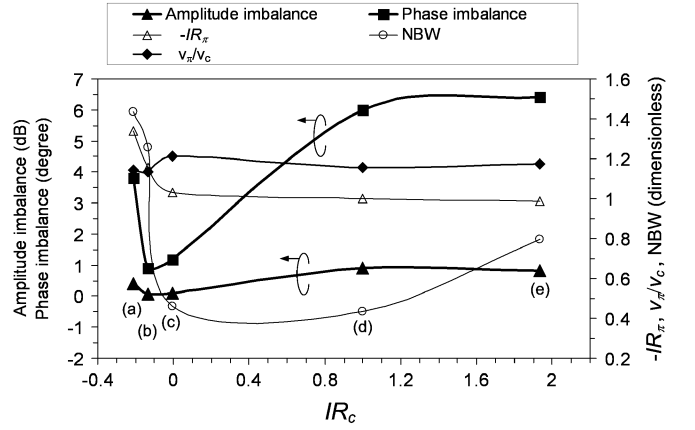


Fig. 7. Phase imbalance versus IR_c -parameter for planar baluns of different structures. (a) Twin-thickness broadside coupled balun. (b) Single-thickness broadside coupled balun. (c) Single-thickness broadside coupled balun with a very wide $W_{ab} = 1842 \mu\text{m}$. (d) Symmetric edge-coupled balun. (e) Asymmetric edge-coupled lines balun.

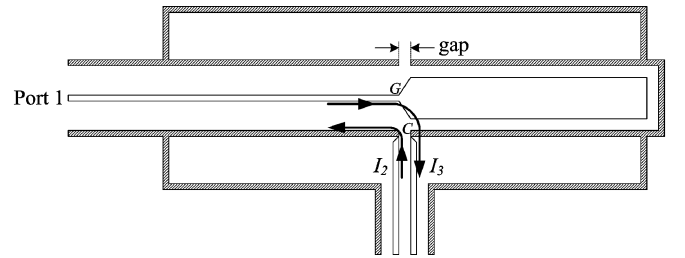


Fig. 8. Original circuit diagram of the coaxial balun by Marchand [1] with the representative flow of currents indicated at center frequency.

B. Detailed Modeling of the Balun

The model originally proposed by Tsai and Gupta [8] based on quasi-static normal mode analysis [15] can be further expanded to include the modeling of secondary effects such as the parasitic inductance of ground via through holes and the stray capacitance across the gap between transmission line Z_a and Z_b . To accurately model phase imbalance of the balun, the extra gap also has to be taken into account since a physical delay will be added to the signal passing through it before reaching port 3 compared to the signal reaching port 2. As shown in Fig. 8, where all transmission lines operate in a dominant TEM mode,

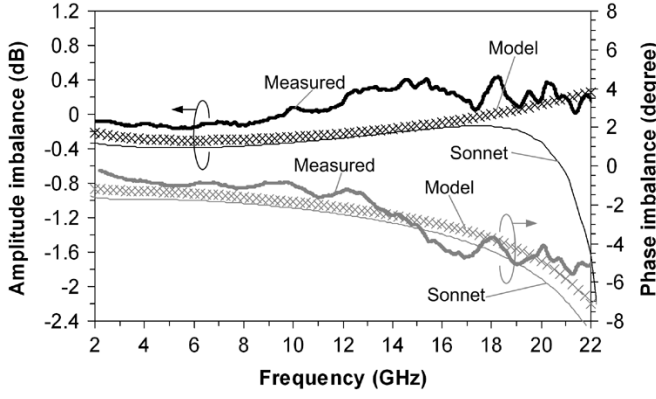


Fig. 12. Measured and modeled amplitude and phase imbalances of a single balun.

TABLE I
PARAMETERS USED IN DETAILED MODEL OF THE BALUN

Parameter	Coupled lines A	Coupled lines B
W (μm)	42	104
L (μm)	3575	3575
H_f (μm)	20	10
R_c (Ω)	1.361	1.518
R_s (Ω)	0.353	0.725
v_c (m/sec)	1.879×10^8	1.867×10^8
v_π (m/sec)	2.085×10^8	1.923×10^8
Z_{cl} (Ω)	-192.5	-37.53
$Z_{\pi l}$ (Ω)	85.23	60.78
θ_c	84.76°	80.44°
θ_π	74.17°	74.65°

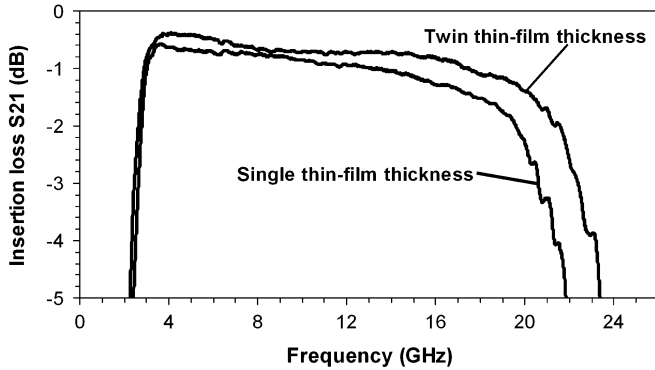


Fig. 13. Measured bandwidth and insertion-loss comparison between a single and twin-thickness thin-film balun. BCB thickness used for the single- and twin-thickness baluns are 10 and 20 μm , respectively.

Amplitude and phase imbalance of the balun are directly calculated from the measured three-port S -parameters of a single balun. The amplitude imbalance is calculated as $\text{dB}(S_{21}) - \text{dB}(S_{31})$, and is smaller than 0.5 dB for 4–20 GHz, as shown in Fig. 12. The phase imbalance is calculated as $180^\circ - |\angle(S_{21}) - \angle(S_{31})|$, and is shown to be less than 5° . The measured and modeled phase and amplitude imbalances are correlated. Table I lists the parameters used in the detailed model for the modeled results plotted out in Figs. 11 and 12. Fig. 13 compares the insertion loss of a balun using twin thin-film thickness versus that using a single thickness. A

conduction loss reduction of 0.5 dB per balun at 20 GHz is achieved with the use of the twin-thickness structure.

B. Time-Domain Measurement

Phase distortion or, equivalently, dispersion across the balun will cause distortion of signals passing through it even as a linear device. Taking the derivative of $\angle S_{21}$ from (2a)–(2c) with respect to frequency leads to a nonzero result, indicating a non-linear phase response and a certain amount of phase distortion even for the ideal TEM balun. The amount of phase distortion is greatest at the lower and higher ends of the passband.

The amount of dispersion can be calculated from the group delay data taken during the S -parameter frequency-domain measurements. Group delay, also known as signal delay and envelope delay, can be written as

$$\tau_g(\omega) = -\frac{\partial \theta}{\partial \omega} \quad (8)$$

where θ is the amount of phase delay over the signal path. Phase constant β is the amount of phase change per unit length, and is expressed as

$$\beta = \frac{\theta}{l} \quad (9)$$

where l is the length of the path. Group velocity is defined as

$$v_g = \left(\frac{\partial \beta}{\partial \omega} \right)^{-1} \quad (10)$$

and the group velocity dispersion (GVD) [18] is a measure of the amount of group velocity variation versus frequency

$$\text{GVD} = \frac{\partial^2 \beta}{\partial \omega^2} = \frac{1}{l} \frac{\partial^2 \theta}{\partial \omega^2}. \quad (11)$$

The widening of a Gaussian pulse with width τ increases with the length traveled l and can be expressed as a function of GVD as [13]

$$\tau' = \sqrt{\tau^2 + \left(\frac{4l}{\tau} \text{GVD} \right)^2}. \quad (12)$$

For small values of GVD and short path lengths of a balun, the amount of Gaussian pulse widening of signals passing through the balun is expected to be nearly zero. Dispersion characteristics and distortion [17] were also confirmed through time-domain measurements to be compared with those predicted and calculated by frequency-domain measurements (Fig. 14). The measurement setup consists of an Agilent E8267C PSG vector signal generator to generate a Gaussian-like modulated pulse input signal into the unbalanced port with the balanced port outputs sampled by an HP 54750A digitizing oscilloscope. The signals have a center frequency swept from 4 to 20 GHz, modulated by the Gaussian-like pulse. The output waveforms are compared to that of a short through line in substitute of the balun under test. The GVD can be back calculated by substituting the difference value back into (12). Time-domain measurement waveforms are plotted out as shown in Fig. 15, indicating an indistinguishable amount of pulse widening and near-zero dispersion.

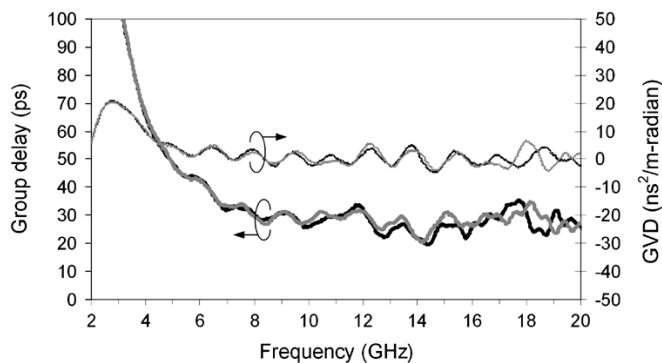


Fig. 14. Group delay and dispersion characteristics predicted from S -parameter measurements of the balun. Black lines show the results for S_{21} , whereas the grey lines show the results for S_{31} .

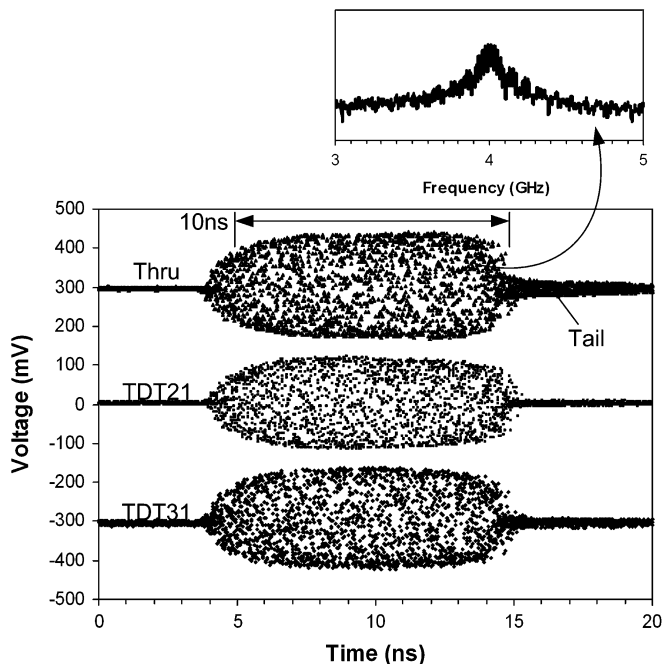


Fig. 15. Digitized waveforms of the balun at the two balanced ports in response to a Gaussian-like modulated input pulse into the unbalanced port. The inset on the upper right corner shows the frequency response of the input modulated pulse centered at 4 GHz. The tail in the waveform is caused by an imperfect turn-off state of the modulating pulse.

VI. CONCLUSION

A planar multilayered Marchand compensated balun has been presented demonstrating a less than 0.7-dB insertion loss throughout the 4–20-GHz specification bandwidth. A proposed multilayered thin-film structure has been successfully employed to reduce the insertion loss without having to sacrifice the balun's bandwidth.

The low insertion loss was achieved by the usage of wide metal traces. Low-cost printed circuit dielectric materials with similar dielectric constants were selected to equalize the c - and π -mode phase velocities and preserve a wide bandwidth. Low amplitude and phase imbalances of 0.5 dB and 5° were achieved through the usage of the multilayered broadside coupled microstrip lines, suppressing the c -mode wave propagation within the transmission lines. The in-band phase imbalance is concluded to be lower for baluns using broadside coupled lines

than for those employing edge-coupled lines. Dispersion has also been characterized and measured to be near-zero for this broad-band balun.

ACKNOWLEDGMENT

The authors wish to thank the reviewers of this paper for their helpful comments. The authors would also like to thank Prof. A. Knoesen and Q. Chen, both with the Department of Electrical and Computer Engineering, University of California at Davis, for their assistance in the time-domain measurements.

REFERENCES

- [1] N. Marchand, "Transmission line conversion transformers," *Electronics*, vol. 17, no. 12, pp. 142–145, Dec. 1944.
- [2] J. W. Lee and K. J. Webb, "A low-loss planar microwave balun with an integrated bias scheme for push-pull amplifiers," in *IEEE MTT-S Int. Microwave Symp. Dig.*, 2001, pp. 197–200.
- [3] J. Schellenberg and H. Do-ky, "Low-loss, planar monolithic baluns for K/K_a -band applications," in *IEEE MTT-S Int. Microwave Symp. Dig.*, vol. 4, Jun. 1999, pp. 1733–1736.
- [4] K. S. Ang, I. D. Robertson, K. Elgaid, and I. G. Thayne, "40 to 90 GHz impedance transforming CPW Marchand balun," in *IEEE MTT-S Int. Microwave Symp. Dig.*, vol. 2, Jun. 2000, pp. 1141–1144.
- [5] M. N. Tutt, H. Q. Tserng, and A. Ketterson, "A low loss, 5.5 GHz–20 GHz monolithic balun," in *IEEE MTT-S Int. Microwave Symp. Dig.*, 1997, pp. 933–936.
- [6] R. Schwindt and C. Nguyen, "Computer-aided analysis and design of a planar multilayer Marchand balun," *IEEE Trans. Microw. Theory Tech.*, vol. 42, no. 7, pp. 1429–1434, Jul. 1994.
- [7] K. Nishikawa, I. Toyoda, and T. Tokumitsu, "Compact and broad-band three-dimensional MMIC balun," *IEEE Trans. Microw. Theory Tech.*, vol. 47, no. 1, pp. 96–99, Jan. 1999.
- [8] C. M. Tsai and K. C. Gupta, "A generalized model for coupled lines and its applications to two-layer planar circuits," *IEEE Trans. Microw. Theory Tech.*, vol. 40, no. 12, pp. 2190–2199, Dec. 1992.
- [9] A. M. Pavio and A. Kikel, "A monolithic or hybrid broad-band compensated balun," in *IEEE MTT-S Int. Microwave Symp. Dig.*, 1990, pp. 483–486.
- [10] R. Bawer and J. J. Wolfe, "A printed circuit balun for use with spiral antennas," *IRE Trans. Microw. Theory Tech.*, vol. MTT-8, no. 3, pp. 319–325, May 1960.
- [11] A. C. Chen, A. Pham, and R. E. Leoni, "Development of a low-loss multilayered broad-band balun using twin-thickness thin film," in *IEEE MTT-S Int. Microwave Symp. Dig.*, Jun. 2005. [CD ROM].
- [12] G. Oltman, "The compensated balun," *IEEE Trans. Microw. Theory Tech.*, vol. MTT-14, no. 3, pp. 112–119, Mar. 1966.
- [13] F. Gardiol, *Microstrip Circuits*. New York: Wiley, 1994.
- [14] W. Janssen, *Hohlleiter Und Streifenleiter*. Heidelberg, Germany: Hüthig, 1977.
- [15] V. K. Tripathi, "Asymmetric coupled transmission lines in an inhomogeneous medium," *IEEE Trans. Microw. Theory Tech.*, vol. MTT-23, no. 9, pp. 734–739, Sep. 1975.
- [16] J. W. Lee and K. J. Webb, "Analysis and design of low-loss planar microwave baluns having three symmetric coupled lines," in *IEEE MTT-S Int. Microwave Symp. Dig.*, vol. 1, Jun. 2002, pp. 117–120.
- [17] D. L. Lee, *Electromagnetic Principles of Integrated Optics*. New York: Wiley, 1986, ch. 10, sec. 6, pp. 301–314.
- [18] G. Keiser, *Optical Fiber Communications*, 3rd ed. New York: McGraw-Hill, 2000, ch. 3.

Andy C. Chen (M'97) received the B.S. degree in electro-physics from National Chiao-Tung University, Taiwan, R.O.C., in 1997, the M.S. degree in electrical engineering from San Jose State University, CA, in 2001, and is currently working toward the Ph.D. degree at the University of California at Davis.

From 1997 to 2003, he was with Atelic Systems Inc., San Jose, CA, as a main CMOS Design Engineer involved in the development of mixed-signal integrated circuits (ICs) and digital signal processors (DSPs). His current research interests include RF integrated circuit (RFIC), microwave, and high-speed digital circuit design and packaging.

Anh-Vu Pham (SM'03) received the B.E.E. (with highest honors), M.S., and Ph.D. degrees from the Georgia Institute of Technology, Atlanta, in 1995, 1997, and 1999, respectively.

In 1997, he cofounded RF Solutions LLC, an RFIC company that was acquired by Anadigics in 2003. He has held faculty positions with Clemson University and the University of California at Davis, where he is currently an Associate Professor. He is also an active consultant to industry. He has authored or coauthored over 50 technical journal and conference papers. His research interests are in the area of RF and high-speed packaging and signal integrity, RFIC design, and wireless sensors.

Dr. Pham serves as a member of the IEEE Microwave Theory and Techniques Society (IEEE MTT-S) International Microwave Symposium (IMS) Technical Program Committee (TPC) on Power Amplifiers and Integrated Circuits. He has been the chair of the IEEE MTT-12 Microwave and Millimeter Wave Packaging and Manufacturing Technical Committee of the IEEE MTT-S. He was the recipient of the 2001 National Science Foundation CAREER Award on millimeter-wave organic packaging.

Robert E. Leoni III (M'98) received the B.S. degree in electrical engineering, B.S. degree in physics, and M.S., and Ph.D. degrees in electrical engineering from Lehigh University, Bethlehem, PA, in 1992, 1993, 1995, and 1998, respectively.

He is currently a Senior Scientist with the RF Components Division, Raytheon Company, Andover, MA. He has authored or coauthored over 30 technical papers. He was the editor of *High Performance Devices—Proceedings of the 2004 IEEE Lester Eastman Conference*.